Numerical demonstration of generation of bound solitons in figure of eight microstructured fiber laser in normal dispersion regime

Faouzi Bahloul, Mohamed Salhi, Khmaies Guesmi, François Sanchez, Rabah Attia

Optics Communications 311 (2013) 282–287

Contents lists available at ScienceDirect

Optics Communications

journal homepage: www.elsevier.com/locate/optcom

Numerical demonstration of generation of bound solitons in figure of eight microstructured fiber laser in normal dispersion regime

Faouzi Bahloul [a,*], Mohamed Salhi [b], Khmaies Guesmi [a,b], François Sanchez [b], Rabah Attia [a]

[a] Laboratoire Systèmes Electroniques et Réseaux de Communications (SERCOM), Ecole Polytechnique de Tunisie, EPT, B.P. 743, 2078, Université de Carthage, Tunisia

[b] Laboratoire de Photonique d'Angers, EA 4464, UFR Sciences, Université d'Angers, 2 Boulevard Lavoisier, FR-49045 Angers Cedex 01, France

ARTICLE INFO

Article history:
Received 28 June 2013
Received in revised form
29 July 2013
Accepted 1 August 2013
Available online 4 September 2013

Keywords:
Figure of eight
Microstructured optical fiber
Split step Fourier method
Bound solitons

ABSTRACT

We have numerically studied passive mode locking in figure of eight laser containing microstructured optical fiber. We demonstrate for the first time to the best of our knowledge the generation of bound states in such configuration in the normal dispersion regime. The numerical simulations are based on extended nonlinear Schrödinger equation using the symmetrized split-step Fourier method. The numerical results show that single pulse or bound solitons can be obtained when the parameters of the cavity are suitably chosen. We identify the small signal gain and the microstructured optical fiber's nonlinear coefficient as key parameters for the generation of bound solitons in figure of eight fiber laser.

1. Introduction

Fiber lasers, which utilize an optical fiber doped with rare earth elements such as erbium or ytterbium as the active gain medium, have been widely investigated in the recent years. Mode locked pulsed fiber lasers have key advantages including high peak power and short pulse duration. Mode locked fiber lasers have found applications in many areas as communication, material processing, biological metrology and medicine [1]. The figure of eight fiber laser is one of the passive laser configurations which allows the generation of the soliton regime. Self-starting passive mode locking in figure of eight laser has been theoretically and experimentally demonstrated [2–6]. The principle of this method is based on the optical Kerr effect. Indeed, nonlinear phase delay between clockwise and counterclockwise waves in a nonlinear optical loop mirror (*NOLM*) or a nonlinear amplifying loop mirror (*NALM*) creates intensity dependent transmission. Both *NOLM* and *NALM* behave like fast saturable absorber.

Two solitons bound state was first theoretically predicted in 1991 by Malomed et al. [7]. The experimental demonstration of a laser delivering two bound pulses was given 10 yr later by Tang et al. [8]. In figure-of-eight lasers the observation of stable bound solitons has been reported in [9]. The bound states were stable over several hours in the laser cavity when no external perturbation is applied. Moreover, the increase of pump power injected in the cavity allowed the generation of bound states of several pulses. The control of the net cavity dispersion was very important to achieve the last regime. Recently, Amrani et al. [10] have shown that various soliton patterns such as a soliton gas, a soliton liquid, a soliton polycrystal and a soliton crystal are directly generated from the figure of eight laser operating in anomalous dispersion. On the other hand, Yun et al. [11] have experimentally obtained dissipative bound state of solitons in figure of eight fiber laser operating in the normal dispersion regime.

Microstructured optical fibers (*MOF*) have attracted much attention since the first demonstration of optical guidance in a *MOF* in 1996 [12]. *MOFs* have shown potential for many practical applications, due to their unique optical properties and have been in the focus of research over the recent years. Light guidance in *MOF* is provided by a periodic arrangement of holes, acting as a cladding, running along the full length of the fiber. A potentially unlimited range of geometric arrangements permits control of optical properties as dispersion, nonlinearity and birefringence [13]. An all-fiber integrated figure-eight laser generating 850 fs pulses at 1065 nm is reported in [14]. In a previous paper, we have investigated the effect of insertion of a *MOF* in figure of eight fiber laser [15]. However, the bound soliton operation of passively mode-locked figure-eight fiber lasers in normal cavity dispersion has not been addressed so far. This was the initial motivation of the work reported in this paper.

In this article, we propose a numerical model of figure of eight microstructured optical fiber laser (*F8MOFL*). The model is based on extended nonlinear Schrodinger (*ENS*) equation and solved

* Corresponding author. Tel.: +216 71 774 611; fax: +216 71 748 843.
E-mail address: faouzi.bahloul@enit.rnu.tn (F. Bahloul).

0030-4018/$ - see front matter © 2013 Elsevier B.V. All rights reserved.
http://dx.doi.org/10.1016/j.optcom.2013.08.002

numerically by using the symmetrised split-step Fourier method (*SSSFM*) [16]. The numerical simulation predicts two pulsed regimes of the laser in normal dispersion. We have identified single pulse regime and soliton pairs regime. Finally, we study the influence of the small signal gain coefficient of *EDFA* and the *MOF's* nonlinear coefficient on the dynamics of pulses generation.

2. Numerical model of figure of eight fiber laser

The cavity design of the passively mode-locked erbium doped fiber laser is schematically shown in Fig. 1. The cavity comprises two loops. The nonlinear amplifying loop mirror (*NALM*) contains erbium doped fiber, microstructured optical fiber, and two pieces of single mode fibers. The unidirectional ring (*UR*) comprises a dispersion shifted fiber (*DSF*) and an optical isolator to ensure unidirectional traveling wave. The optical power is extracted from a 80/20 fiber coupler.

We investigate the dynamic of pulse propagation in *F8MOFL* by using numerical simulations. The cavity is modeled as a sequence of different elements with specific characteristics. We treat each element separately and take the solution obtained after propagation in the considered element as the initial condition for the next one. This situation is close to reality. In our calculation we consider an input field with intensity $|E_{in}|^2$ at the port 1 of the central coupler.

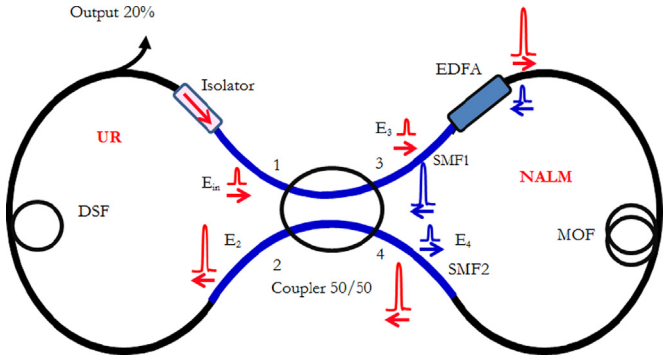

Fig. 1. Setup of the figure of eight microstructured optical fiber laser.

It is split into two counter propagating fields $E_3=\sqrt{0.5}E_{in}$ and $E_4=j\sqrt{0.5}E_{in}$.

The pulse evolution in the *NALM* is determined by the propagation of the fields E_3 and E_4. They propagate in the *NALM* in the clockwise and counterclockwise direction as illustrated in Fig. 2(a) and (b).

For simplicity, we assume in our approach that all fields are linearly polarized and that the fibers do not modify the polarization of the traveling waves. That means that neither natural birefringence nor nonlinear coupling between the polarization eigenstates is considered. We can therefore use a scalar model for the field propagation. Under such condition, the optical pulse propagation through the *EDFA* is governed by the extended nonlinear Schrödinger equation [17]:

$$\frac{\partial E}{\partial z}+j\left(\frac{\beta_2}{2}+j\frac{g}{2\omega_g^2}\right)\frac{\partial^2 E}{\partial T^2}-\frac{g-\alpha}{2}E=j\gamma|E|^2E \tag{1}$$

where E is the complex envelop of the electric field, z is the propagation distance, β_2 is the second order fiber dispersion, α is the linear absorption coefficient. $\gamma=2\pi n_2/\lambda A_{eff}$ is the nonlinear parameter of the fiber where n_2 is the nonlinear index associated to the optical Kerr effect, λ the optical wavelength and A_{eff} the effective mode area. T is the delayed time ($T=t-z/v_g$), v_g is the group velocity and g is the saturated gain expressed by

$$g=\frac{g_0}{1+(E_p/E_s)} \tag{2}$$

where g_0 is the small signal gain (or unsaturated gain proportional to the pumping power), E_p is the pulse energy, $E_s=1$ pJ is the saturation energy and $\omega_g=15.7$ ps^{-1} is the spectral gain bandwidth.

For the undoped fibers, g is taken equal to zero. We have used *SSSFM* for solving *ENS* equations modeling the propagation of the pulse in the *F8MOFL*. The method is illustrated in Fig. 3. It includes the effects of second order dispersion, spectral gain filtering in the amplifier, linear losses, saturable gain and self-phase modulation. *ENS* equation, taking into the account the last effects, is written in a more compact way by using linear $\hat{D}$ and nonlinear $\hat{N}$ operators

$$\frac{\partial E}{\partial z}=(\hat{D}+\hat{N})E \tag{3}$$

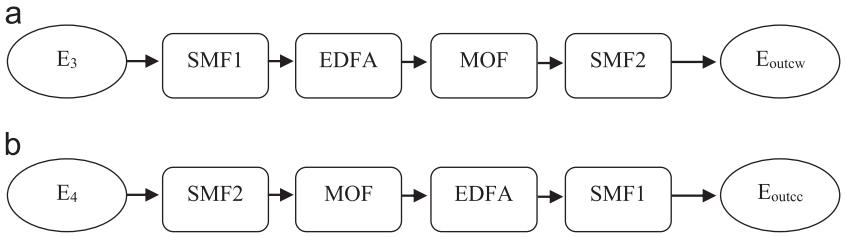

Fig. 2. General schematic of the *NALM* model (a) in the clockwise direction (b) in the counterclockwise direction (E_{outcw}, E_{outccw} are electric fields traveling in the clockwise and counterclockwise directions, respectively).

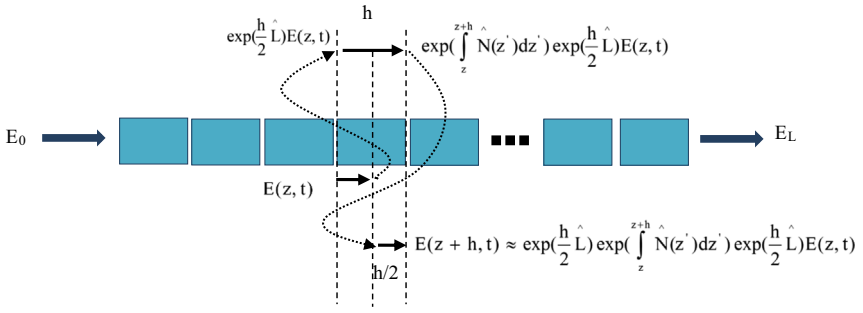

Fig. 3. Symmetrized split step Fourier algorithm.

$$\hat{D} = -j\left(\frac{\beta_2}{2} + j\frac{g}{2\omega_g^2}\right)\frac{\partial^2}{\partial T^2} - \frac{\alpha}{2} \tag{4}$$

$$\hat{N} = j\gamma|E|^2 + \frac{g}{2} \tag{5}$$

The amplitude of the transmitted field in port 2 after the propagation in the *NALM* is

$$E_2 = \sqrt{0.5}E_{outccw} + j\sqrt{0.5}E_{outcw}, \tag{6}$$

We use the last field as the input field for the *UR* cavity. The optical isolator is also considered and easily implemented by the computational procedure. The computed output field of the *UR* cavity is then used as the new input for the *NALM*. This iterative procedure is repeated until a steady-state is achieved. Our model takes into account the effect of localized cavity components unlike the conventional master equation method widely used to simulate the operation of soliton lasers [17,18].

3. Results and discussions

Pulse characteristics and shape at each round trip of *F8MOFL* were recorded and analyzed. The pulses were plotted together in time domain. This gives an idea of how the pulse evolves as a function of the number of cavity rounds trips. Numerical simulations of the laser operation are undertaken to give a qualitative behavior and a physical description of the pulse generation. They are carried out by considering an initial Sech profile pulse and propagating it through the various components shown in Fig. 1. The peak power of the injected Sech pulse is 1 W and its duration (*FWHM*) is 5 ps. In order to avoid the soliton energy quantization effect occurring in the soliton regime the total dispersion is set in the normal regime with $\beta_2^{TOT}L = 0.021$ ps^2. The total cavity length is L=41 m corresponding to a round trip time of 205 ns and to a fundamental repetition rate of 4.9 MHz. Parameters used in our simulations are listed in Table 1.

Table 1
Parameters used in the simulations.

Property	$SMF_{1,2}$	*DSF*	*MOF*	*EDFA*
L (m)	2	2	20	15
α (dB/km)	0.2	0.2	0.2	0.5
γ (W^{-1} km^{-1})	1.25	1.25	10.5	2.35
β_2 (ps^2/km)	−21.6	140.2	−22.9	19.1

The numerical results are reported in Fig. 4 which give the evolution of the input Sech profile pulse. It is demonstrated the formation of a stable self-starting single pulse as short as 800 fs with 4.7 pJ pulse energy. If the steady state is established after a given number round trips (10 in this case) in the cavity it remains stable over all numbers of round-trip period tested numerically.

3.1. Effect of small signal gain

With appropriate net group dispersion, and through increasing the pump power, which in our model corresponds to increase the small signal gain coefficient (g_0), self-starting mode locked laser is automatically obtained in our simulations as shown in Fig. 4. Fig. 5 gives the evolution of the pulse energy as a function of the small signal gain. As one could easily expect, the energy increases when g_0 increases. When g_0 is less than 0.5 m^{-1}, there is no mode locking. In the experiment this corresponds to the case where the laser is below the mode locking threshold. Mode locking starts for $g_0 = 0.5$ m^{-1}. While g_0 is further increased, the pulse energy quickly increases and reaches the value of 5.3 pJ which appears

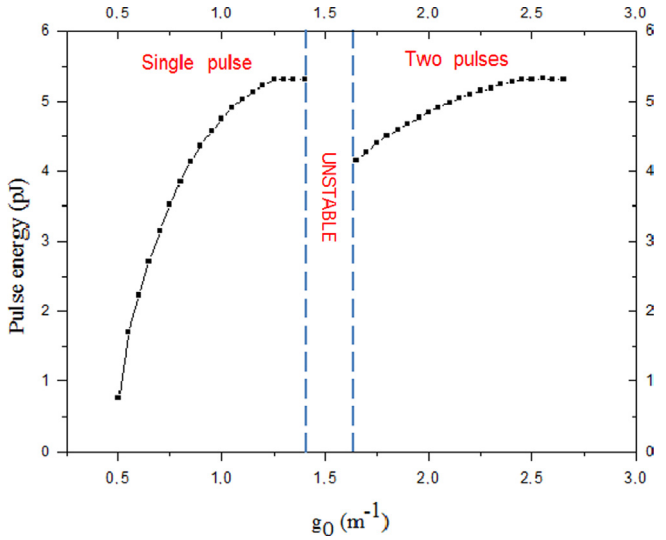

Fig. 5. Evolution of pulse energy versus small signal gain.

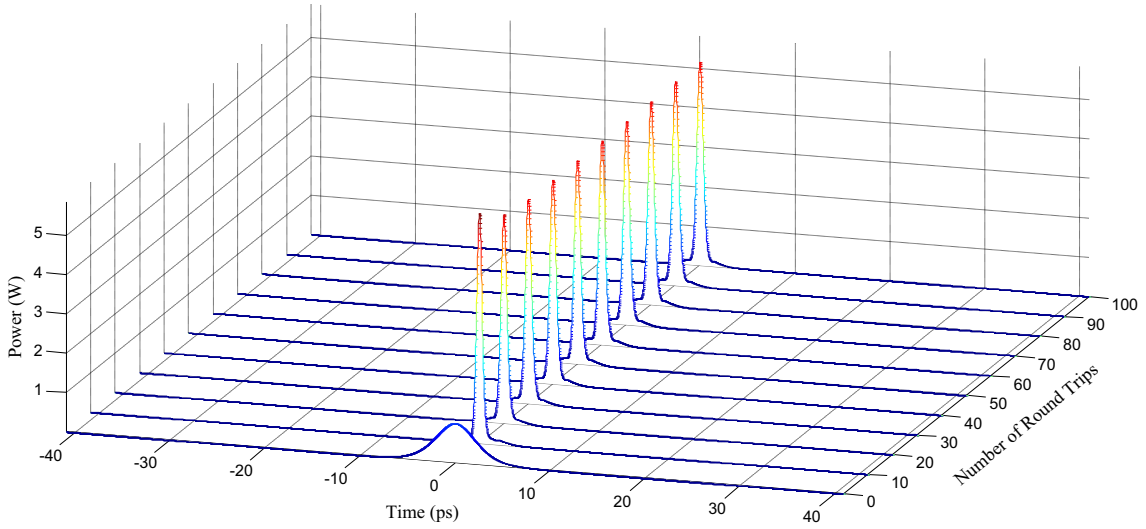

Fig. 4. Single pulse generation in *F8MOFL* for $g_0 = 1$ m^{-1}.

as a saturation value. This energy saturation is directly connected to the transmission of the *NALM*. Indeed, while the transmission of the *NALM* first increases when g_0 increases because of constructive interferences between the contra-propagative waves, the increase of the nonlinear dephasing leads progressively to less constructive interferences and then to a saturation of the energy. For $1.45\ \mathrm{m}^{-1} \le g_0 \le 1.65\ \mathrm{m}^{-1}$ no stable mode-locking is numerically obtained. This region corresponds to the transition between single-pulse and double-pulse emission; it is also related to the nonlinear transmission of the *NALM* which is very low for high intensities thus leading to less favorable conditions for mode-locking. In order to point out the role of the nonlinear filtering of the *NALM* on the multiple pulsing, we have plotted in Fig. 6 the evolution of the transmission of the *NALM*, defined as $T_{NALM} = \int |E_2(T)|^2 dT / \int |E_{in}(T)|^2 dT$, as a function of the small signal gain g_0. For the calculation of the transmission we have chosen input pulse characteristics in agreement with data of Fig. 4, i.e. a pulse width (*FWHM*) of 830 fs and a variable energy, keeping in mind that for the data of Fig. 4 the energy of the pulse incident on the *NALM* is about 19 pJ. Results show that T_{NALM} is below unity for $g_0 \le 0.5$ thus meaning that losses of the whole cavity cannot be compensated by the *NALM*; the laser is below threshold and no laser operation occurs. Above this value, T_{NALM} increases and the energy of the pulse also. Then T_{NALM} decreases and the energy of the pulse saturates. When T_{NALM} approaches its minimum, again losses are not compensated and no mode-locking regime is possible; this corresponds to the unstable region in Fig. 5. When g_0 is further increased, T_{NALM} recovers values allowing the mode-locked regime to occur. In this region, a second pulse appears as a

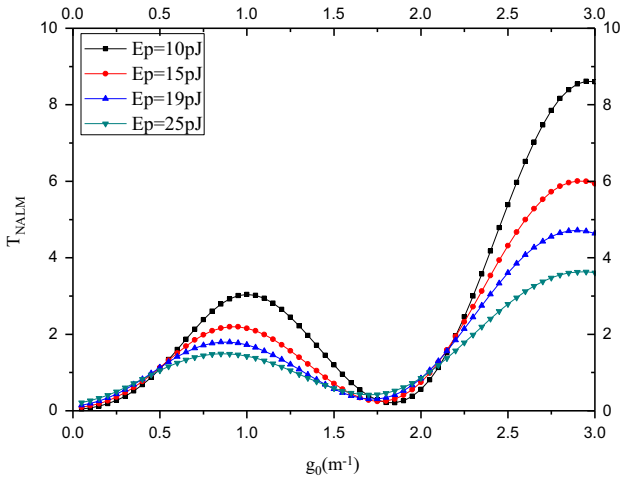

Fig. 6. Evolution of the nonlinear transmission of the *NALM* versus small signal gain for different input pulse energy.

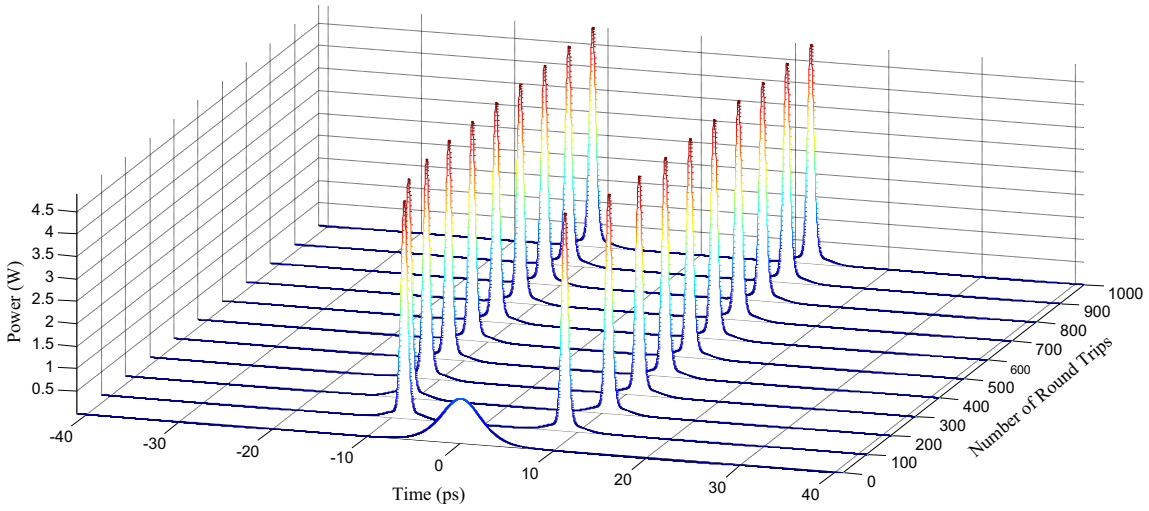

Fig.7. Bound state generation in *F8MOFL* for $g_0 = 2\ \mathrm{m}^{-1}$.

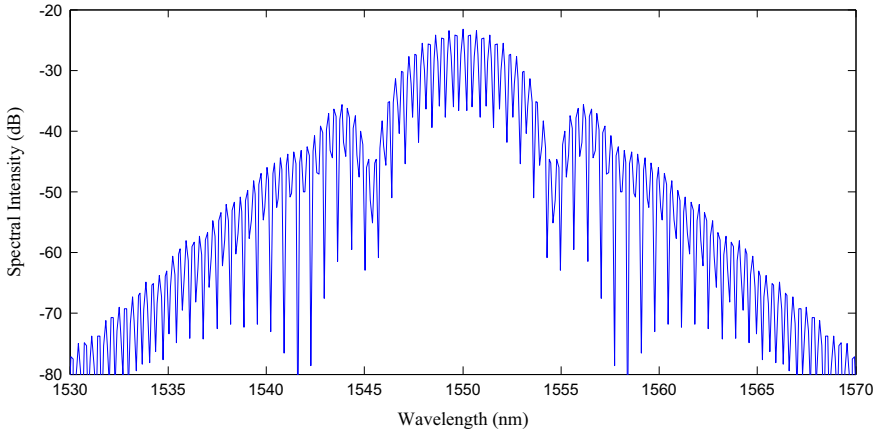

Fig. 8. Optical spectrum of bound solitons.

result of the pulse energy saturation imposed by the *NALM*. Of course, the interpretation given above is only qualitative because when the cavity is closed, the energy of the input pulse on the *NALM* depends on g_0 while it is not the case in our simple transmission analysis.

For $g_0 \geq 1.65\ \mathrm{m}^{-1}$, the pulse will split into two pulses with energy per pulse ≈ 4 pJ. The two pulses have a same shape as in the single pulse regime. Fig. 7 shows an example of bound solitons obtained at $g_0 = 2\ \mathrm{m}^{-1}$ after 400 round trips in the cavity. The time separation between the two solitons is 23 ps. Each pulse is characterized by duration of 800 fs and energy per pulse of 5.1 pJ. Additional analyses are performed in Fig. 8 concerning the optical spectrum averaged on several round trips. It reveals a modulation which proves that there is a constant phase relation between the two solitons thus confirming that they form a bound state. The spectral modulation period is 0.35 nm, which corresponds to the same soliton separation obtained in temporal domain (see Fig. 7). We attributed the formation of this regime to direct interactions between two solitons. The bound solitons is independent of the initial conditions which indicate that this regime can be achieved from noise for the specific parameters. These numerical results favorably compare with the experimental observations [9]. On the other hand, these results are very important from a practical point of view because they mean that the amplifying medium is mainly responsible for the emergence of several pulses in the normal dispersion regime.

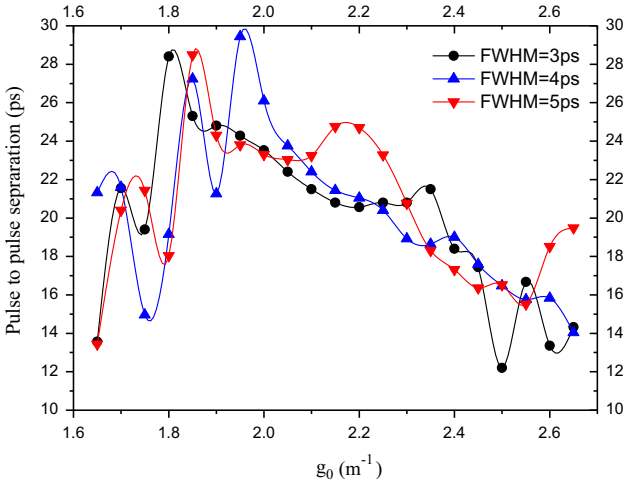

Fig. 9. Pulse to pulse separation versus g_0.

Table 2
Effect of changing of initial conditions on pulse to pulse separation.

Width (ps)	Pulse to pulse separation (ps)
1	21.2
2	19.4
3	23.5
4	26.1
5	23.3

Let us now consider the influence of the small signal gain on the delay between the two solitons. Results are shown in Fig. 9 in the range of g_0 for which bound states occur. In contrast with the evolution obtained in fiber lasers passively mode-locked through nonlinear polarization evolution [19], the delays do not seem quantified. Indeed there is no clear evolution of the delay between solitons. For example, the smallest separation, obtained for $g_0 = 1.65\ \mathrm{m}^{-1}$, is *13* ps while the largest separation is 28 ps for $g_0 = 1.85\ \mathrm{m}^{-1}$ considering one initial pulse (or two initial pulses) with peak power=1 W and *FWHM*=5 ps. In order to study the effect of changing of initial conditions on pulse to pulse separation, we vary distance between two initial pulses and their width (see Fig. 9). By injecting two pulses (peak power=1 W, *FWHM*=3, 4 and 5 ps and distance between two initial pulses=60 ps), we remark that pulse to pulse separation is independent on the distance between two initial pulses but is dependent of their width. Table 2 presents an example obtained for $g_0 = 2\ \mathrm{m}^{-1}$ and for a distance between two initial pulses of 60 ps.

3.2. Effect of MOF's nonlinear coefficient

Let us now study the effect of *MOF's* nonlinear coefficient (γ) on pulse parameters evolution. We change γ from 1.3 to $10.5\ \mathrm{W}^{-1}\ \mathrm{km}^{-1}$ corresponding to effective mode area A_{eff} which varies from 80 to $10\ \mu\mathrm{m}^2$. Fig. 10 shows the evolution of the steady-state output intensity for increasing values of A_{eff}. High *MOF's* nonlinear coefficient leads to strong nonlinear effects. Results show that while A_{eff} decreases, first the pulse energy increases and then the pulse splits into two pulses. This illustrates the fact that excessive nonlinearity can have very detrimental effects. It often limits the achievable pulse energy. If we replace the *MOF* by *SMF* we obtain single pulse with 2.65 pJ pulse energy.

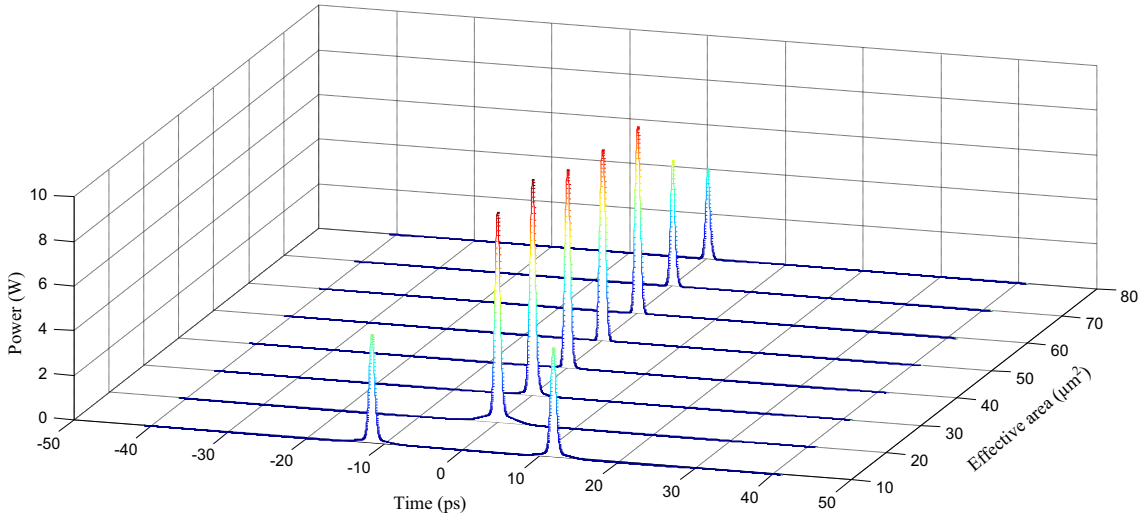

Fig. 10. Effect of effective area on pulse generation for $g_0 = 2\ \mathrm{m}^{-1}$.

When the energy exceeds 9.4 pJ, we obtain two pulses. These results prove that the pulse shape is dependent on the *MOF's* nonlinear coefficient. Finally, we predict, for the first time to the best of our knowledge, the generation of bound soliton pairs in the normal dispersion regime by *NALM* figure of eight fiber lasers.

4. Conclusion

In summary, we have numerically studied properties of bound-soliton emission in a passively mode-locked figure of eight micro-structured fiber laser in normal dispersion regime. We have found that the small signal coefficient of *EDFA* and *MOF's* nonlinear coefficient play important roles in the formation of soliton pairs. The laser operates in the single-pulse state when the small signal gain is low, whereas it delivers bound-state pulses for higher values of the small signal gain. In between, there is no stable mode-locking.

References

[1] N. Li, J. Xue, C. Ouyang, K. Wu, J.H. Wong, S. Aditya, P.P. Shum, Applied Optics 51 (17) (2012) 3726.
[2] V. Tzelepis, S. Markatos, S. Kalpogiannis, T.H. Sphicopoulos, C. Caroubalos, Journal of Lightwave Technology 11 (11) (1993) 1729.
[3] I. Duling, OSA Technical Digest Series (1990)PDP8.
[4] T.G. Sindhu, Prem B. Bisht, R.J. Rajesh, M.V. Satyanarayna, Microwave and Optical Technology Letters 28 (3) (2001) 196.
[5] M. Salhi, A. Haboucha, H. Leblond, F. Sanchez, Physical Review A 77 (2008) 033828.
[6] M. Salhi, F. Amrani, H. Leblond, F. Sanchez, Physical Review A 82 (2010) 043834.
[7] B.A. Malomed, Physical Review A 44 (1991) 6954.
[8] D.Y. Tang, W.S. Man, H.Y. Tam, P.D. Drummond, Physical Review A 64 (2001) 033814.
[9] N.H. Seong, D.Y. Kim, Optics Letters 27 (15) (2002) 1321.
[10] F. Amrani, M. Salhi, P. Grelu, H. Leblond, F. Sanchez, Optics Letters 36 (9) (2011) 1545.
[11] L. Yun, Laser Physics 23 (2013) 045106.
[12] P. St., J. Russel, Journal of Lightwave Technology 24 (12) (2006) 4729.
[13] S. Haxha, H. Ademgil, Optics Communications 281 (2008) 278.
[14] A.V. Avdokhin, S.V. Popov, J.R. Taylor, Optics Express 11 (2003) 265.
[15] T. Ennejah, F. Bahloul, M. Salhi, R. Attia, Journal of Optical Communications 35 (2013) 1.
[16] G.P. Agrawal, Nonlinear Fiber Optics, Academic, Boston, 1989.
[17] T. Schreiber, B. Ortaç, J. Limpert, A. Tünnermann, Optics Express 15 (13) (2007) 8252.
[18] H.A. Haus, J.G. Fujimoto, E.P. Ippen, Journal of the Optical Society of America B 8 (1991) 2068.
[19] A. Komarov, K. Komarov, F. Sanchez, Physical Review A 79 (2009) 033807.